ISSN 1330-3651 (Print), ISSN 1848-6339 (Online) https://doi.org/10.17559/TV-20230626000761
Preliminary communications

Design of Single-phase PWM Rectifier Based on PI Double-loop Control

Kezhou BAI, Qushan CHEN*

Abstract: In this paper, the mathematical model of PWM rectifier is analyzed first, and the rotating coordinate system transformation is used to convert the mathematical model to frequency domain, and the control model is established through the frequency domain model. Since the *d*-axis and *q*-axis currents are coupled with each other, this paper adopts the current feedforward processing to decouple the current loop, and introduces the PI regulator as the main control link between the current loop and the voltage loop to obtain the control models of the current inner loop and the voltage outer loop. In this paper, the current inner loop control model and the voltage outer loop control model are simulated in Simulink, and root locus analysis and Bode diagram analysis are used to first determine the parameters of the current inner loop within the expected range of the relevant parameters, and then determine the parameters of the voltage outer loop by the control model of the current inner loop. A double-loop control system with better performance is finally derived.

Keywords: decouple; double-loop control; rotating coordinate system transformation; single-phase PWM rectifier

1 INTRODUCTION

The rapid evolution of power electronics has led to the application of PWM control technology in various types of power converters. Compared with traditional rectifiers, there are numerous advantages of PWM rectifiers, such as limited input current harmonics, high energy return rate and low volume filter [1, 2]. Single-phase PWM (Pulse Width Modulation) rectifiers are widely used in modern production and life, with simple circuit structure, flexible design and high efficiency of variable current. Single closed-loop control has the disadvantages of slow response, weak interference immunity, and poor robustness [3]. In order to ensure the stability of the system and improve the dynamic performance, most of the traditional single-phase PWM rectifiers use a double-loop control method based on current inner loop and voltage outer loop [4]. The current loop control is divided into two methods: direct current control and indirect current control, where direct current control methods mainly include *d-q* current decoupling control [5], PID control, hysteresis control [6] and PR control [7]. Direct current control has advantages of good current waveform and fast dynamic response [8]. It is difficult to achieve the steady-state zero error requirement by traditional PID control alone. Hysteresis loop control has problems such as uncontrollable switching frequency and large losses.

In this paper, the current control method based on rotating coordinate system is proposed through the conventional double-loop control [9] model of a single-phase PWM rectifier, which can convert AC to DC in a synchronous rotating coordinate system. It has high flexibility, which can arbitrarily control the magnitude of the reactive current measured by the rectifier AC and realize the output of high power factor on the network side.

This paper consists of five sections. The first section introduces the research object of this paper. The second section establishes the control model of single-phase PWM rectifier by coordinate conversion and feedforward decoupling. The third section designs the parameters of the controller by root locus and Bode plot. The fourth section simulates and verifies in Simulink. The fifth section summarizes the paper and proposes the next work plan.

2 ANALYSIS OF CONTROL SYSTEM PRINCIPLES

2.1 Mathematical Model

The subject of this study is the single-phase PWM rectifier circuit indicated in Fig. 1. The input voltage *U*s is 24 V AC, the output voltage *U*dc is 50 V DC, the inductor value is L = 1158 μH, the internal resistance is r = 0.4 Ω, the capacitor value is C = 2000 μF, and the output load is R = 40 Ω. Angular frequency of the input AC voltage is ω = 100π rad/s.

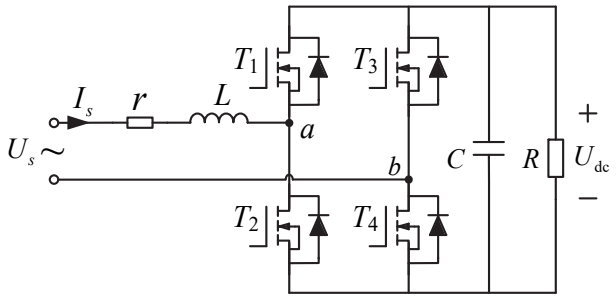

Figure 1 Single-phase PWM rectifier circuit topology

Firstly, the mathematical model of the electrical part is developed according to the circuit analysis [10], as in Eq. (1).

$$\left.\begin{aligned} L\frac{\mathrm{d}i_\mathrm{s}}{\mathrm{d}t} &= u_\mathrm{s} - ri_\mathrm{s} - Su_\mathrm{dc} \\ C\frac{\mathrm{d}u_\mathrm{dc}}{\mathrm{d}t} &= Si_\mathrm{s} - \frac{u_\mathrm{dc}}{R} \end{aligned}\right\} \tag{1}$$

where S is the PWM wave modulation ratio, which can be obtained from values of the input and output voltage:

$$S = \frac{24\sqrt{2}}{50} = 0.6788 \tag{2}$$

Conversion of AC variables to direct flows in *d-q* coordinate system using PLL (Phase Locked Loop) and Park transform:

$$\left.\begin{aligned} L\frac{\mathrm{d}i_{\mathrm{sd}}}{\mathrm{d}t} &= u_{\mathrm{sd}} - ri_{\mathrm{sd}} - u_{\mathrm{abd}} + \omega Li_{\mathrm{sq}} \\ L\frac{\mathrm{d}i_{\mathrm{sq}}}{\mathrm{d}t} &= u_{\mathrm{sq}} - ri_{\mathrm{sq}} - u_{\mathrm{abq}} - \omega Li_{\mathrm{sd}} \end{aligned}\right\} \tag{3}$$

In single-phase voltage-type PWM rectifiers, static and rotating coordinate system transformations are defined in order to convert the difficult-to-control AC quantities into easily controllable direct flows, and the transformation vector control diagram of the rotation coordinate system is shown in Fig. 2 below.

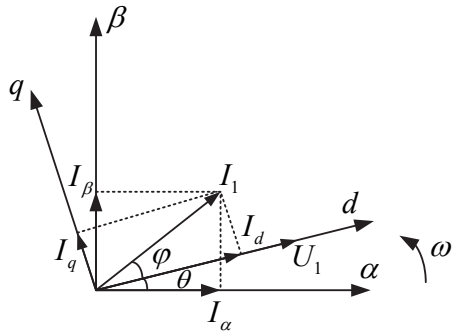

Figure 2 Transformation of stationary to rotating coordinate system

The relationship between two coordinate systems is as follows [11]:

$$\begin{bmatrix} i_d \\ i_q \end{bmatrix} = \begin{bmatrix} \cos\theta & \sin\theta \\ -\sin\theta & \cos\theta \end{bmatrix} \begin{bmatrix} i_\alpha \\ i_\beta \end{bmatrix} \tag{4}$$

The mathematical model of Eq. (3) describes the model of the current variation in the *d-q* coordinate system. In automatic control principles, instead of parameter design in the time domain, the mathematical model is usually converted to the frequency domain, thus simplifying the calculation. Converting the above equation to the s-domain, we have:

$$\left.\begin{aligned} U_{\mathrm{abd}}(\mathrm{s}) &= U_{\mathrm{sd}}(\mathrm{s}) - (sL+r)\cdot I_{\mathrm{sd}}(\mathrm{s}) + \omega LI_{\mathrm{sq}}(\mathrm{s}) \\ U_{\mathrm{abq}}(\mathrm{s}) &= U_{\mathrm{sq}}(\mathrm{s}) - (sL+r)\cdot I_{\mathrm{sq}}(\mathrm{s}) - \omega LI_{\mathrm{sd}}(\mathrm{s}) \end{aligned}\right\} \tag{5}$$

2.2 Control Block Diagram

The mathematical model of Eq. (5) is translated into a flow block diagram, as shown in Fig. 3.

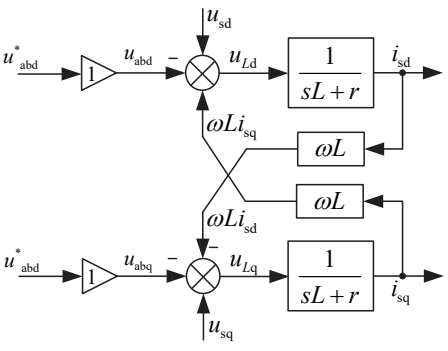

Figure 3 Block diagram of the flow of current change after *d-q* conversion

From this model, it can be seen that the currents in *d-q* axis are coupled to each other, which is not conducive to the individual control of *d-q* axis currents, so the current feedforward is decoupled before the rectifier control. As in Eq. (6):

$$\left.\begin{aligned} U_{\mathrm{abd}} &= U_{\mathrm{sd}} + \omega LI_{\mathrm{sq}} - (K_{\mathrm{p}} + \frac{K_{\mathrm{i}}}{s})\cdot(I^*_{\mathrm{sd}} - I_{\mathrm{sd}}) \\ U_{\mathrm{abq}} &= U_{\mathrm{sq}} - \omega LI_{\mathrm{sd}} - (K_{\mathrm{p}} + \frac{K_{\mathrm{i}}}{s})\cdot(I^*_{\mathrm{sq}} - I_{\mathrm{sq}}) \end{aligned}\right\} \tag{6}$$

where I^*_{sd} and I^*_{sq} are the target values of I_{sd} and I_{sq}. From Eq. (5) and Eq. (6), it is obtained that:

$$\left.\begin{aligned} (sL+r)\cdot I_{\mathrm{sd}} &= (K_{\mathrm{p}} + \frac{K_{\mathrm{i}}}{s})\cdot(I^*_{\mathrm{sd}} - I_{\mathrm{sd}}) \\ (sL+r)\cdot I_{\mathrm{sq}} &= (K_{\mathrm{p}} + \frac{K_{\mathrm{i}}}{s})\cdot(I^*_{\mathrm{sq}} - I_{\mathrm{sq}}) \end{aligned}\right\} \tag{7}$$

It can be seen that I_{sd} and I_{sq} are decoupled and completely symmetrical. Therefore, the *d-q* current loop can be designed independently, and the control parameters are exactly the same, so the block diagram of the current inner loop is derived, as shown in Fig. 4.

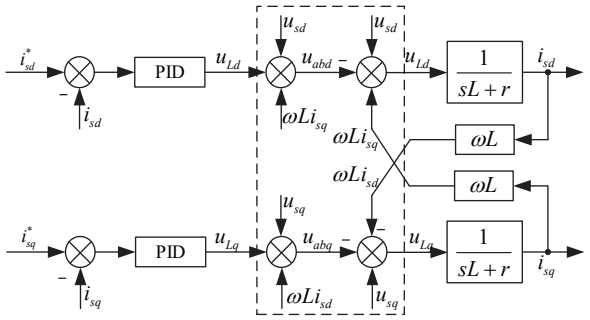

Figure 4 *d-q* axis current feedforward decoupling model diagram

After the electrical part is modeled, a PI controller is introduced to control the output current. The difference between current actual value of the current and reference value of the voltage loop output is used as the input to PI controller, and the output is the *d-q* component of the inductor voltage U_{Ld} and U_{Lq}.

According to the model of current feedforward decoupling in Fig. 4, the block diagram of current control is obtained i_{sd} and i_{sq} shown in Fig. 5.

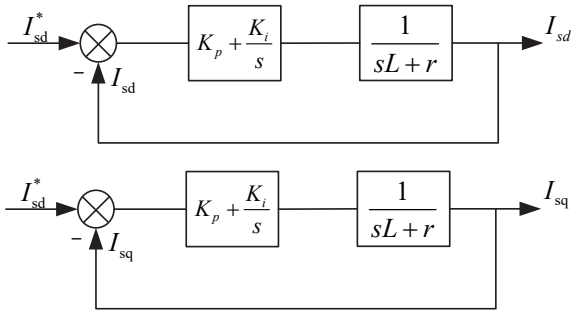

Figure 5 Block diagram of current inner loop control

From Fig. 5, the open-loop transfer function and the closed-loop transfer function of the current inner loop are obtained as follows:

$$G_{i\text{op}} = (K_{\text{Ip}} + \frac{K_{\text{Ii}}}{s}) \cdot \frac{1}{sL + r} \tag{8}$$

$$G_{i\text{cl}} = \frac{I_{\text{sd}}^*}{I_{\text{sd}}} = \frac{I_{\text{sq}}^*}{I_{\text{sq}}} = \frac{K_{\text{Ip}} + \frac{K_{\text{Ii}}}{s}}{sL + r + K_{\text{Ip}} + \frac{K_{\text{Ii}}}{s}} \tag{9}$$

K_{Ip} and K_{Ii} are the current loop PI parameters respectively. Adding voltage loop to control the output DC voltage at 50 V, the block diagram of the double-loop control system is shown in Fig. 6.

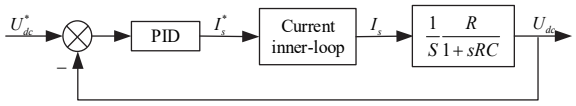

Figure 6 Voltage external loop voltage stabilization control

The open-loop transfer function (Eq. (10)) and closed-loop transfer function (Eq. (11)) of voltage and current double-loop are obtained and the complete block diagram of the control system is shown in Fig. 7.

$$G_{\text{op}} = (K_{\text{p}} + \frac{K_{\text{i}}}{s}) \cdot G_{i\text{cl}} \cdot \frac{1}{S}\frac{1}{1 + sRC} \tag{10}$$

$$G_{\text{cl}} = \frac{U_{dc}^*}{U_{dc}} = \frac{(K_{\text{p}} + \frac{K_{\text{i}}}{s}) \cdot G_{i\text{cl}}}{(K_{\text{p}} + \frac{K_{\text{i}}}{s}) \cdot G_{i\text{cl}} + (1 + sRC) \cdot S} \tag{11}$$

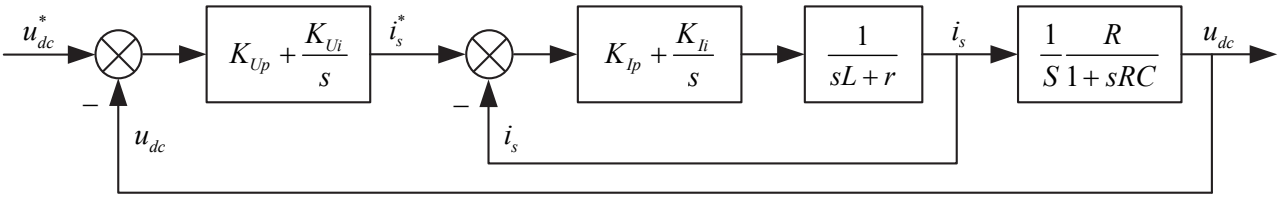

Figure 8 Rectifier master control block diagram

3 CONTROLLER PARAMETERS DESIGN

3.1 Performance Analysis

The PI regulator takes into account the rapidity and reduces or eliminates the static difference. The PD regulator has the regulation static difference, which is suitable for large hysteresis links [12]. The PID controller responds faster to changes in the control input, allowing the control signal to be increased so that the steady-state error is zero, eliminating oscillations [13].

The system described in this topic has no large hysteresis links, requires a faster response, eliminates static errors as much as possible, and for safety reasons, cannot have too much overshoot. To sum up, PI regulator is chosen as the controller of this topic.

Before the introduction of PI regulator, the system is a series connection of two first-order inertial systems, so the current loop and voltage loop are engineered to control these two first-order inertial systems, with the current loop as the inner loop while the voltage loop as the outer loop.

To test the performance of the closed-loop parameters, the most extreme case should be considered, i.e., when the input signal is a step signal, the step response curve of the system is examined, and optimal PI parameters are determined based on its overshoot, regulation time, and other parameters [14].

When designing the voltage outer loop, the target performance is: PM (Phase Margin) at 40-50 degrees; Overshoot amount at 15%-20%; 2% regulation time within.

The above target performance is for the step response. In the actual application of the system, the change of the reference value will be much smaller than the step response, so system response time and oscillation will be significantly less.

3.2 Controller Parameter Design

3.2.1 Design of Current Inner Loop Parameters

First, the Evens form of the open-loop transfer function of the current inner loop:

$$G_{i\text{op}} = \frac{K_{\text{Ip}}}{L} \cdot \frac{s + \frac{K_{\text{Ii}}}{K_{\text{Ip}}}}{s(s + \frac{r}{L})} \tag{12}$$

From this, the open-loop zero point can be determined as $-K_{\text{Ii}}/K_{\text{Ip}}$, and the open-loop poles as 0 and $-r/L$. When the zero point is located between the two poles, the root locus coincides with the real axis, at this time the dominant pole does not contain the imaginary axis component, the response overshoot PO adjustable range is small and cannot meet the design requirements.

When the zero point is located on the left side of the two poles, the root locus is distributed within the real and imaginary axes, and the damping ratio of the system can be changed by changing the angle of the imaginary axis between the dominant pole and the origin line to adjust the response overshoot PO at 15%-20% to meet the design requirements.

To obtain a faster response, the open-loop zero point is arranged to the left of the two poles, so there is a constraint:

$$\frac{K_{\text{Ii}}}{K_{\text{Ip}}} > \frac{r}{L} = 345.423 \tag{13}$$

Select K_{Ii}/K_{Ip} = 2200. In order to make the overshoot *PO* in 15%-20%, the closed-loop pole of the appropriate *PO* corresponding to the damping ratio is selected on the root locus, and this closed-loop pole is brought into closed-loop transfer function to find K_{Ip} = 0.125, K_{Ii} = 275.

Using MATLAB to plot root locus of the open-loop transfer function (Fig. 8) with Bode diagram (Fig. 9), the overshoot *PO* = 19.2% and PM is 49.6°, both of which meet the requirements.

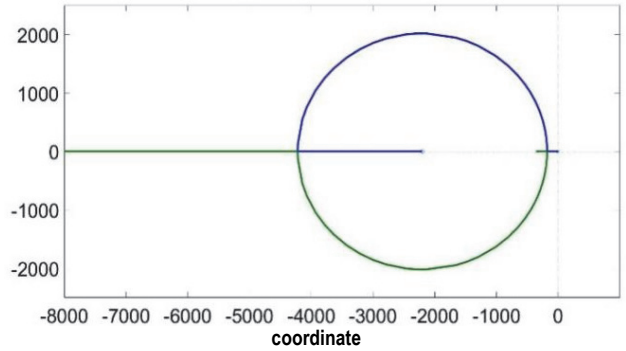

Figure 8 Root locus diagram of current inner loop

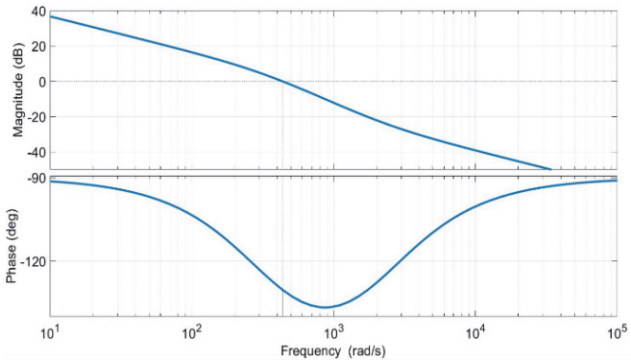

Figure 9 Bode diagram of the current inner loop

3.2.2 Design of Voltage Outer Ring Parameters

The open-loop transfer function of the voltage outer loop derived from Eq. (10) is written and simplified to Eq. (14).

$$G_{op} = \frac{(sK_p + K_i)}{s} \cdot \frac{R(sK_{Ip} + K_{Ii})}{S(1+sRC)[s^2L + s(K_{Ip} + r) + K_{Ii}]} \quad (14)$$

Plotting its root locus, omitting the non-dominant zero poles, the open-loop transfer function can be simplified to Eq. (15).

$$G_{op} = \frac{(sK_p + K_i)}{s} \cdot \frac{R}{S(1+sRC)} \quad (15)$$

This is a first-order inertial system with the addition of a PI correction link, analogous to the current inner loop. A similar idea is used to design the current inner loop parameters, which are selected K_i/K_p =425.

In order to keep the overshoot *PO* at 15%-20%, the closed-loop pole of the appropriate *PO* corresponding to the damping ratio is selected on the root locus, and this closed-loop pole is brought into the closed-loop transfer function to obtain K_p = 0.0013, K_i = 0.5525.

Using MATLAB to plot root locus of the open-loop transfer function (Fig. 10) and the Bode diagram (Fig. 11), the overshoot *PO* = 19.4% and the PM is 48.7°, both of which meet the requirements.

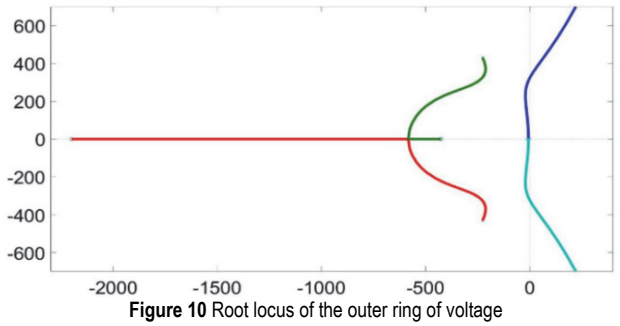

Figure 10 Root locus of the outer ring of voltage

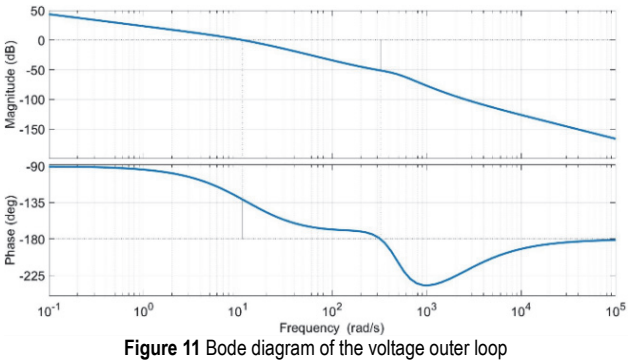

Figure 11 Bode diagram of the voltage outer loop

4 SIMULATION VERIFICATION

4.1 Introduction of Simulation Model

4.1.1 Simulink Modelling of Electrical Section

According to Fig. 1, the simulation circuit is built in Simulink as Fig. 12. The input voltage is 24 Vrms, 50 Hz AC, the circuit contains four MOS tubes, and the output voltage is under the control of the modulation ratio of the SPWM wave, and the output voltage is observed using an oscilloscope.

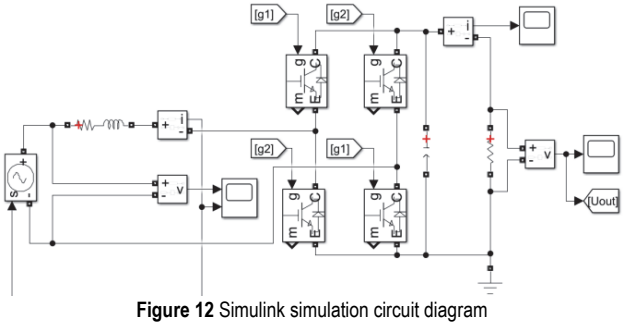

Figure 12 Simulink simulation circuit diagram

4.1.2 Simulink Modelling of Control Section

As shown in Fig. 13 the input current I_s is *d-q* transformed, and the transformed I_{sd} and I_{sq} are PI controlled and feedforward decoupled respectively, and then *d-q* inverse transformed to obtain the SPWM wave modulation ratio, and the SPWM modulation wave controls the MOS tube opening and closing, and the output half-bridge midpoint voltage U_{ab}.

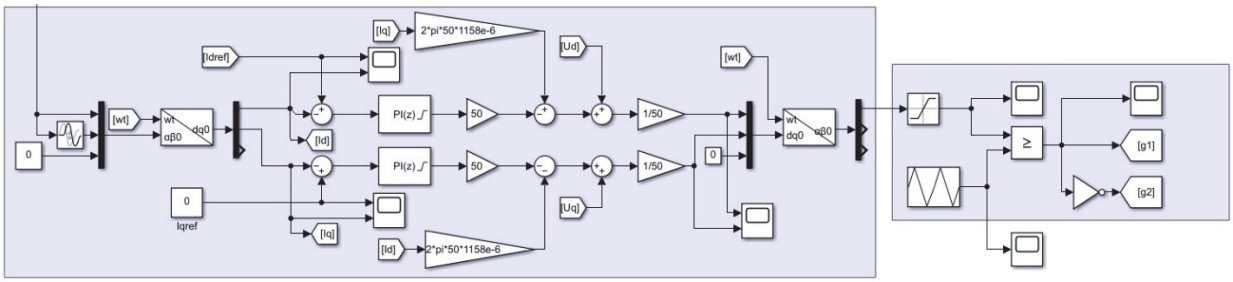

Figure 13 Current inner loop control with SPWM modulation section

The voltage reference is 50 V and the PI control results in a reference value for the current shown in Fig. 14.

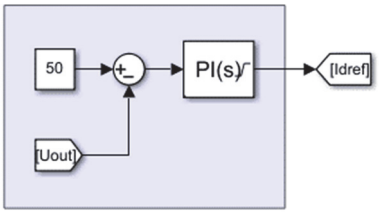

Figure 14 Simulation circuit voltage outer loop control

The PLL phase-locking algorithm is used to obtain the θ required for the *d-q* transformation, and then the *d-q* components of the input voltage and input current are calculated based on this shown in Fig. 15.

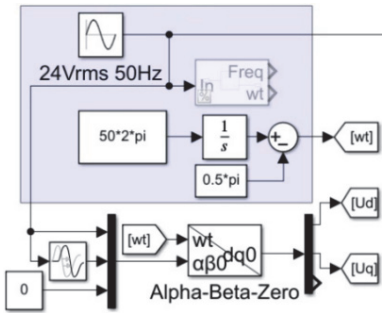

Figure 15 Simulation of phase-locked loop and *d-q* conversion in a circuit

4.2 Simulation Waveforms and Data

The double-loop control block diagram in Simulink is shown in Fig. 7 for the voltage loop and the current loop in Fig. 16.

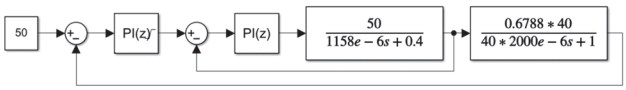

Figure 16 Block diagram of double-loop control built by simulation

The step signal is input and the step response waveform of the system is obtained as shown in Fig. 17.

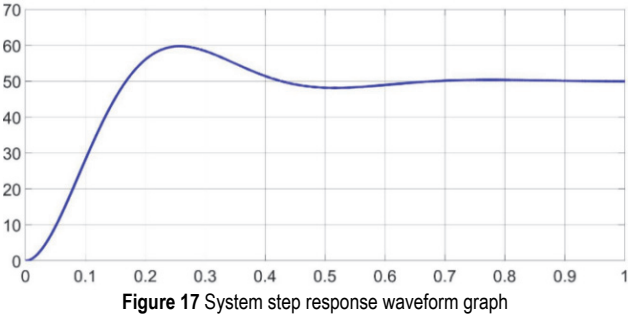

Figure 17 System step response waveform graph

As shown in Fig. 17, $PO = 19.44\%$, $T_s = 0.613$ s, which meets the performance requirements.

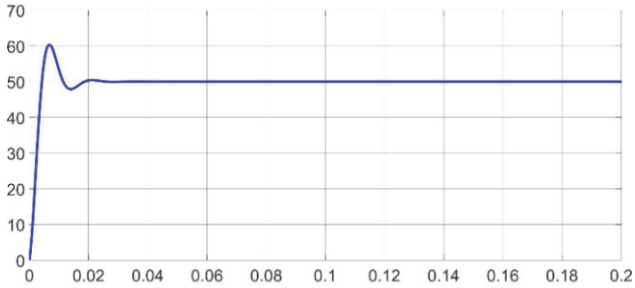

Figure 18 Current inner loop step response simulation curve

As seen in Fig. 18, the 2% regulation time of the current inner loop is 16.324 ms, which is much smaller than the response time of the voltage outer loop, so the system can respond better.

4.3 Analysis of Simulation Results

Substituting the double closed-loop parameters from Section 4.1 into the control model, the output DC voltage waveform is obtained by running Simulink simulation as shown in Fig. 19.

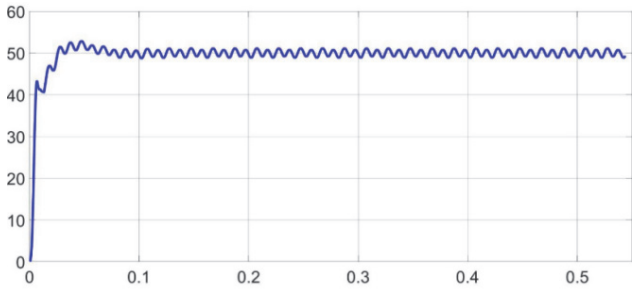

Figure 19 Simulink simulation results of output voltage

The step response curve overshoot of the system is *PO* = 19.44% and the regulation time. For this subject, the output DC voltage should follow the input quantity change as fast as possible and reach the steady state quickly, so a certain amount of overshoot is allowed to exist.

Observing the waveform diagram obtained from the circuit simulation model, the output voltage is able to reach the set value of 50 V relatively quickly and contains a high frequency harmonic component of 100 Hz. This is due to the inherent defect of the voltage-based PWM rectifier. In order to filter out the 100 Hz ripple component in the feedback signal and to ensure the fast response of the overall loop, a low-pass filter is introduced in the voltage

loop to ensure that noise signals at 100 Hz are filtered out without affecting the high frequency characteristics [15].

Alternatively, a predictive controller with repeatable learning can be used as the current inner loop while adding a digital trap filter to the voltage outer loop to suppress harmonics and improve the power factor [16].

5 CONCLUSION

In this paper, we start from the electrical and mathematical model of PWM rectifier circuit, simplify the model by coordinate conversion, and introduce PI control link to establish the control model of rectifier. Additionally, the parameters of the regulator are obtained within the expected range of performance parameters by using the analysis of root locus and Bode diagram. Lastly, models of the circuit and control system are established in Simulink, and it is verified that the dynamic property of the rectifier response is favorable while the steady-state property is consistent with the requirements under the design parameters. The conclusions are summarized as follows:

1) The feedforward decoupling and coordinate conversion used in this paper realize the independent control of voltage and current and provide a simplified method for complex control models. These two control methods can be widely used in double-loop control systems where voltage and current are coupled with each other.
2) The control model established in this paper for single-phase PWM rectifier is universal. According to the conclusion of this paper, the control model under different design conditions can be obtained by changing the parameters.
3) Simulation results obtained in SIMULINK illustrate the advantages of double-loop control with excellent dynamic response, no static difference, and high stability, proving that the double-loop control method can lead to a better performance of the power converter.

In order to further verify the characteristics of the control system designed in this paper, it is required to build an experimental platform for testing. The next step in the research should more carefully consider the potential effects of actual single-phase PWM rectifiers, such as the switching frequency of the MOS, the modulation of the PWM, the EMI of the system, etc. The control system is required to be tested under non-ideal conditions and the PI parameters of the control system should be further optimized based on the actual situation.

6 REFERENCES

[1] Wei, X. (2003). The PWM unity power factor rectifier based on space vector. *Electric drive*, *4*, 40-43.

[2] Wei, X., Liu, Z., & Wang, N. (2003). Unit power factor rectifier based on space voltage vector pulse width modulation. *Electric Drive*, 40-43.

[3] Chen, X., Shen, B., Chen, D., Zeng, X., Zhou, F., & Li, L. (2017). The three-phase unbalanced overvoltage suppression method based on double-loop PI control for distribution network. *2017 IEEE Conference on Energy Internet and Energy System Integration (EI2)*, 1-5. https://doi.org/10.1109/EI2.2017.8245436

[4] Kim, Y. C., Jin, L., Lee, J., & Choi, J. (2010). Direct Digital Control of Single-Phase AC/DC PWM Converter System. *Journal of Power Electronics*, *10*(5), 518-527. https://doi.org/10.6113/JPE.2010.10.5.518

[5] Salaet, J., Alepuz, S., Gilabert, A., Bordonau, J., & Peracaula, J. (2002). D-Q modeling and control of a single-phase three-level boost rectifier with power factor correction and neutral-point voltage balancing. *2002 IEEE 33rd Annual IEEE Power Electronics Specialists Conference*, 514-519.

[6] Dahono, P. A. (2009). New hysteresis current controller for single-phase full-bridge inverters. *IET Power Electronics*, 585-594. https://doi.org/10.1049/iet-pel.2008.0143

[7] Zmood, D. N. & Holmes, D. G. (2003). Stationary frame current regulation of PWM inverters with zero steady-state error. *IEEE Transactions on Power Electronics*, 18(3), 814-822. https://doi.org/10.1109/TPEL.2003.810852

[8] Yang, Y. & Jie, H. (2007). Design of Voltage PWM Rectifier Controller. *Modern Electronics Technique*, 170-171+188.

[9] Bhagiya, R. D. & Patel, R. M. (2019). PWM based Double loop PI Control of a Bidirectional DC-DC Converter in a Standalone PV/Battery DC Power System. *2019 IEEE 16th India Council International Conference (INDICON)*, 1-4. https://doi.org/10.1109/INDICON47234.2019.9028974

[10] Zhang, X. (2003). *Research on PWM rectifier and its control strategy*. PhD dissertation, Hefei University of Technology, China.

[11] Wu, B. (2018). *Research on three-phase voltage PWM rectifier*. Master thesis, Anhui University of Technology, China.

[12] Nikhar, A. R., Apte, S. M., & Somalwar, R. (2016). Review of various control techniques for DC-DC interleaved boost converters. *2016 International Conference on Global Trends in Signal Processing, Information Computing and Communication (ICGTSPICC)*, 432-437. https://doi.org/10.1109/ICGTSPICC.2016.7955340

[13] Priya, T. H., Parimi, A. M., & Rao, U. M. (2016). Development of hybrid controller for photovoltaic based DC-DC boost converter in DC grid connected applications. *2016 International Conference on Circuit, Power and Computing Technologies (ICCPCT)*, 1-6. https://doi.org/10.1109/ICCPCT.2016.7530221

[14] Majhi, S. & Atherton, D. P. (1999). Autotuning and controller design for processes with small time delays. *IEE Proceedings - Control Theory and Application*s, 415-425. https://doi.org/10.1049/ip-cta:19990433

[15] Awaar, V. K., Rani, M. N. S., Kirthi, D. K., Sindhu, C., Samanvita, P., & Keerthana, P. S. (2022). Implementation of Digital Filters to Improve Dynamic Response of a Single Phase PWM Rectifier. *2022 IEEE 2nd International Conference on Sustainable Energy and Future Electric Transportation (SeFeT)*, 1-6. https://doi.org/10.1109/SeFeT55524.2022.9908997

[16] Wang, C., Zou, Y., Zhang, Y., Xu, Y., She, X., & Li, F. (2008). Research on the single-phase PWM rectifier based on the repetitive control. *2008 IEEE International Conference on Industrial Technology*, 1-6.

Kezhou BAI
School of Electrical and Electronic Engineering,
Huazhong University of Science and Technology, Wuhan, China

Qushan CHEN
(Corresponding author)
School of Electrical and Electronic Engineering,
Huazhong University of Science and Technology, Wuhan, China
E-mail: chenqushan@hust.edu.cn; 13503767971@163.com